ACSNANO

www.acsnano.org

ARTICLE

Atomic Layers of Graphene for Microbial Corrosion Prevention

Govind Chilkoor, Namita Shrestha, Alex Kutana, Manoj Tripathi, Francisco C. Robles Hernández, Boris I. Yakobson, Meyya Meyyappan, Alan B. Dalton, Pulickel M. Ajayan,* Muhammad M. Rahman,* and Venkataramana Gadhamshetty*

Cite This: *ACS Nano* 2021, 15, 447−454

Read Online

ACCESS | Metrics & More | Article Recommendations | Supporting Information

ABSTRACT: **Graphene is a promising material for many biointerface applications in engineering, medical, and life-science domains. Here, we explore the protection ability of graphene atomic layers to metals exposed to aggressive sulfate-reducing bacteria implicated in corrosion. Although the graphene layers on copper (Cu) surfaces did not prevent the bacterial attachment and biofilm growth, they effectively restricted the biogenic sulfide attack. Interestingly, single-layered graphene (SLG) worsened the biogenic sulfide attack by 5-fold compared to bare Cu. In contrast, multilayered graphene (MLG) on Cu restricted the attack by 10-fold and 1.4-fold compared to SLG-Cu and bare Cu, respectively. We combined experimental and computational studies to discern the anomalous behavior of SLG-Cu compared to MLG-Cu. We also report that MLG on Ni offers superior protection ability compared to SLG. Finally, we demonstrate the effect of defects, including double vacancy defects and grain boundaries on the protection ability of atomic graphene layers.**

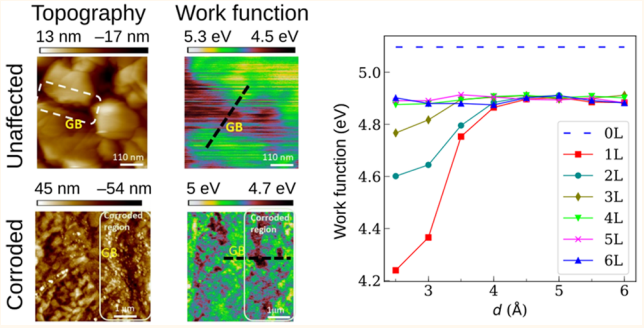

KEYWORDS: *biofilms, defects, graphene, microbial corrosion, density-functional theory, sulfate-reducing bacteria*

Microorganisms cause nearly 20% of corrosion failures, resulting in ∼$2.5 billion of the global corrosion costs annually.[1] For instance, biofouling, biogenic sulfide attack, or microbiologically influenced corrosion (MIC)[2] issues caused by sulfate-reducing bacteria (SRB) require the US Navy to spend ∼$1 billion every year. SRB is a major bacterial group that directly or indirectly challenges the structural integrity of metals by producing highly reactive and corrosive agents including sulfide species. Compared to planktonic (floating) cells, their sessile counterparts (biofilms) are 1000 times more resistant to biocides and induce 100-fold greater corrosion. Although polymer coatings based on polyurethane, epoxy, and polyamides can protect metals from abiotic corrosion,[3] they are susceptible to biodegradation under aqueous conditions.

Owing to the quantum confinement effects at the nanoscale, atomic graphene layers have been found to display many outstanding properties that may be useful in protecting metals exposed to aggressive biological environments. Graphene offers high mechanical strength (1100 GPa), impermeability,[4,5] and hydrophobicity.[1] It has shown oxidation resistance to metals[6] in ambient conditions[7] as well as to aggressive chlorides,[8] boiling seawater,[9] acids,[10] oxidizers,[11] and humidity.[12] Also, atomic layers of graphene can protect nanostructured metals from oxidation.[13,14] For instance, transparent electrodes based on a copper nanowire−graphene core−shell nanostructure showed better thermal oxidation and chemical stability due to the tight encapsulation of the copper nanowire within graphene shells. Another study showed that the direct 3D coating of the graphene layer on interlacing copper nanosilks network electrodes achieved high transparency and robust antioxidant ability.[15] Graphene can be combined with functional groups as well as other 2D materials to create heterostructures that are more resistant in biological environments. Thus, graphene has been considered to control *in vitro*/*in vivo* behavior of many biological systems.[16,17]

Despite many pending challenges, chemical vapor deposition (CVD) remains the most effective method for manufacturing high-quality, large-area graphene.[18,19] Here, we prepared atomic graphene layers by CVD and explored them as

Received: May 13, 2020
Accepted: December 22, 2020
Published: December 31, 2020

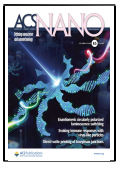

https://dx.doi.org/10.1021/acsnano.0c03987
ACS Nano 2021, 15, 447−454

protective coatings on copper (Cu) exposed to anoxic sulfate-rich biological environment simulated by a genetically tractable *Desulfovibrio alaskensis* G20 (DA-G20) strain. We studied MIC of Cu corrosion as it is a prevalent problem in many engineering applications (*e.g.*, corrosion of canisters used to store nuclear wastes). Although Cu is stable under abiotic conditions,[20] SRB renders it susceptible to corrosion even under ambient conditions.[21] We assessed the quality of as-grown single-layered graphene (SLG) and multilayered graphene (MLG) coatings using microscopy and spectroscopy techniques. We then used electrochemical methods to quantify the degree of biogenic sulfide attack and biotic corrosion. We found that atomic graphene layers neither restrict the growth of DA-G20 cells nor the biofilm. However, SLG on Cu worsens the biogenic sulfide attack by 5-fold compared to bare Cu. In contrast, the MLG forms an impermeable barrier to protect the Cu surface from aggressive metabolites released by the biofilm. The MLG-Cu restricts the biogenic sulfide attack by 10-fold and 1.4-fold compared to SLG and bare Cu, respectively. We combined experimental and computational studies to explain the effect of structural properties of atomic graphene layers on the biogenic sulfide attack. We also studied the graphene layers on nickel substrates to discern their protection behavior on other metals. Finally, we studied the effect of double vacancy defects and grain boundaries on the protection ability of atomic graphene layers.

RESULTS AND DISCUSSION

We synthesized SLG (~1 layer) and MLG (~8 layers) on 25 μm thick Cu substrates using low-pressure CVD techniques, as described in our previous studies.[22] In typical experiments, methane (35 sccm) was delivered to the CVD chamber at 1000 °C and 500 mTorr. MLG was grown using a CH_4/H_2 mixture (10:30 sccm) at atmospheric pressure and 940 °C for 20 min. The graphene films on Cu formed continuous sheets in both SLG and MLG samples, as shown in Figure 1a,c, respectively. The wrinkles across the Cu grain boundaries corroborate the continuity of graphene films. For further characterization by optical imaging, Raman, and TEM analysis, we transferred the films from Cu foil onto SiO_2/Si substrates using a poly(methyl methacrylate) (PMMA)-assisted method.[23] The SLG sample reflected a consistent spread of light blue tint on the light pink background of SiO_2/Si (Figure 1b); the MLG sample displayed a varying film thickness, evident from patches of light blue within the large bright blue background (Figure 1d). The Raman spectra for both samples exhibited a G band and 2D band corresponding to the E_{2g} vibration mode at 1590 and 2665 cm^{-1}, respectively (Figure 1e,f). The G/2D ratio for SLG and MLG was in the range of 0.5−0.6 and 1.7−1.9, indicating single-layered and multi-layered graphene, respectively. The D band in SLG and MLG indicates the presence of defects and disorders.[24,25] The TEM images confirmed one and eight atomic layers in SLG and MLG, respectively (Figure 1g). Finally, the water contact angle values for Cu, SLG-Cu, and MLG-Cu were 82.3° ± 2.0°, 92.2° ± 2.0°, and 94.2° ± 3.0°, respectively (Figure 1h−j), which agree with previous studies.[26]

An immediate application of as-grown graphene atomic layers is their use as a coating to protect underlying Cu surfaces from an aggressive biogenic sulfide attack. We found that the atomic graphene layers neither restricted the cell attachment nor biofilm growth, as shown in the SEM images (Figure 2a). Upon a prolonged exposure for 8 days, the cells grew into a

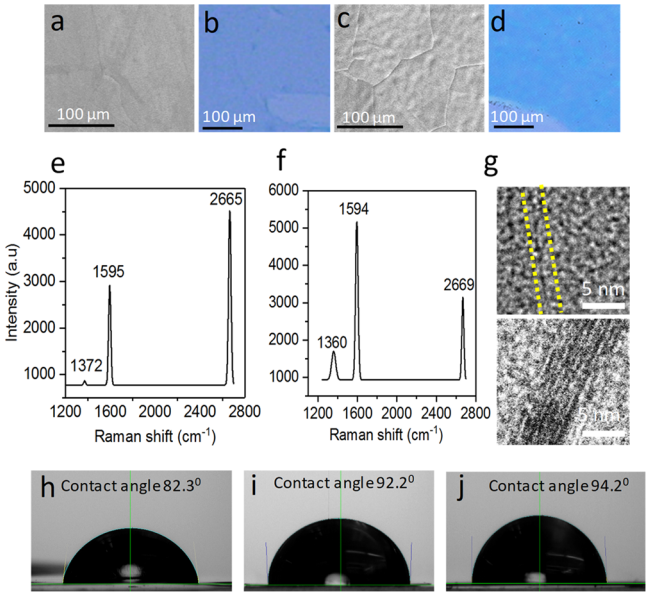

Figure 1. (a,c) SEM images of single-layered graphene (SLG) and multilayer graphene (MLG) on Cu substrate. (b,d) Corresponding optical images of the transferred SLG and MLG films on SiO_2/Si substrates, respectively (background color). (e,f) Corresponding Raman spectra of SLG and MLG, respectively. SLG and MLG display a sharp G band (~1590 cm^{-1}) and 2D band (~2660 cm^{-1}), respectively. The G/2D ratio was 0.6 and 1.6, respectively. (g) TEM image of folded edge shows SLG (top) and MLG (~8 layers) (bottom). (h−j) Static water contact angle values for bare Cu, SLG-Cu, and MLG-Cu, respectively.

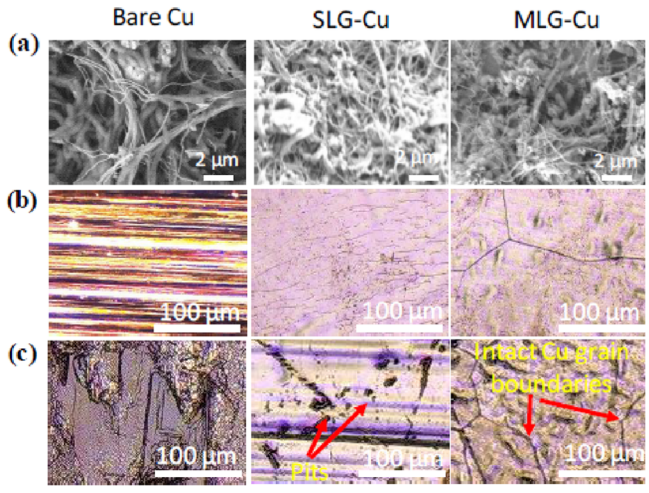

Figure 2. (a) SEM images of SRB DA-G20 biofilm growth on bare Cu, SLG-Cu, and MLG-Cu. (b) Optical images of bare Cu, SLG-Cu, and MLG-Cu before the exposure. (c) Optical images of bare Cu, SLG-Cu, and MLG-Cu after 8 days of exposure. SLG-Cu developed intense pitting corrosion (pits shown as red arrows) and bare Cu inherited signatures of the uniform corrosion (copper sulfide corrosion products displaced in black color). MLG-Cu stayed intact.

matured biofilm containing typical rod-shaped cells of DA-G20 on both the layered surfaces. This finding comes as a surprise in light of the recent studies on antimicrobial properties of CVD-graphene/Cu, specifically to *Escherichia coli* (*E. coli*) and *Staphylococcus aureus* (*S. aureus*).[27] In a subsequent study, Novoselov and co-workers confirmed that graphene materials

https://dx.doi.org/10.1021/acsnano.0c03987
ACS Nano 2021, 15, 447−454

neither stimulate nor inhibit the growth of *E. coli* and *S. aureus*.[28] The artifact on the antimicrobial properties of graphene is due to the presence of impurities in graphene.[28]

As expected, bare Cu experienced a significant biogenic sulfide attack, as confirmed by the XRD peaks of copper sulfides (Cu_2S) (Figure S1, Supporting Information). Surprisingly, SLG-Cu experienced a higher degree of microbial attack, confirmed by more intense sulfide peaks (Figure S1). We used ASTM-G1 protocols to remove the corrosion deposits and microbial debris from the Cu surfaces to visualize the degree of attack on the actual Cu surface with optical image analysis. As shown in Figure 2c, the SLG-Cu developed a rough topography, darker shades of corrosion products, and the localized pitting (black colored pits shown by red arrows). SLG-Cu inherited a pronounced signature of MIC compared to bare Cu (Figure 2c). In contrast, the MLG-Cu surface remained intact with visible Cu grain boundaries (Figures 2b,c). These results suggest that SLG-Cu aggravated the microbial attack while MLG-Cu offers outstanding protection in biological environments.

Next, we used electrochemical methods to quantify the biotic corrosion behavior of bare and coated Cu surfaces (Figure 3). SLG-Cu experienced an accelerated degree of Cu

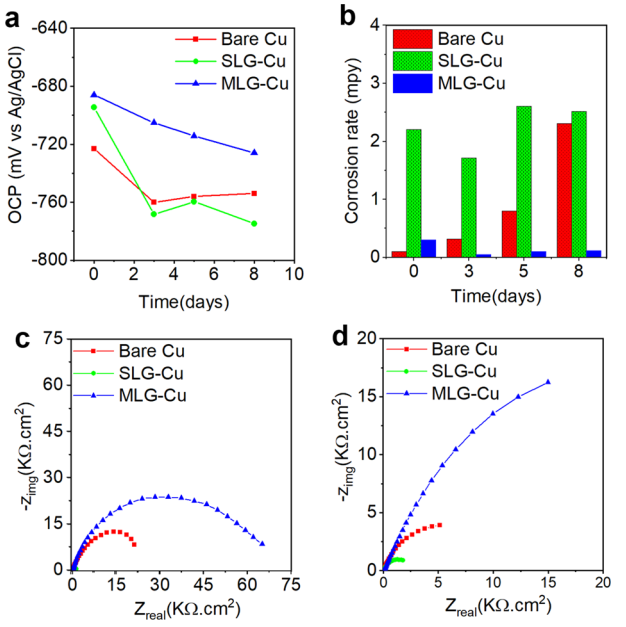

Figure 3. Temporal variation of (a) open-circuit voltage and (b) corrosion rates for 8 days of exposure period to DA-G20. Nyquist plots on (c) day 0 (planktonic, t < 2 h) and (d) day 8 using a sinusoidal AC potential of 10 mV in the frequency range of 0.01−10^5 Hz.

dissolution, as evident from the downward trend (more negative values) of the open-circuit potential (OCP) compared to bare Cu (Figure 3a); this downward trend was sustained for the entire exposure period. The lower polarization resistance (R_p) values of SLG-Cu corroborate its worsened corrosion behavior (Figure S2). For instance, the R_p for SLG-Cu on day 3 was 80% lower than bare Cu. Finally, the corrosion rates of SLG-Cu on day 0 and day 8 were ∼22-fold and 5-fold higher than bare Cu, respectively (Figure 3b). In contrast, MLG layers on Cu offered biotic corrosion resistance, as evident from their positive OCP values (−715 mV *vs* Ag/AgCl) compared to Cu (−760 mV *vs* Ag/AgCl) as well as SLG-Cu (−776 mV *vs* Ag/AgCl). The R_p value for MLG-Cu on day 3 was 7 times and 36 times higher compared to those of bare Cu and SLG-Cu, respectively (Figure S2). The MLG-Cu suppressed the Cu dissolution by 95% when compared to bare Cu.

We used a computational study based on density functional theory to understand the worsened biotic corrosion behavior of SLG-Cu compared to bare Cu and MLG-Cu. The inherent structural defects in graphene[29] layers (depicted as one- to six-atom vacancies, V_1 to V_6 in Figure 4a) constitute potential

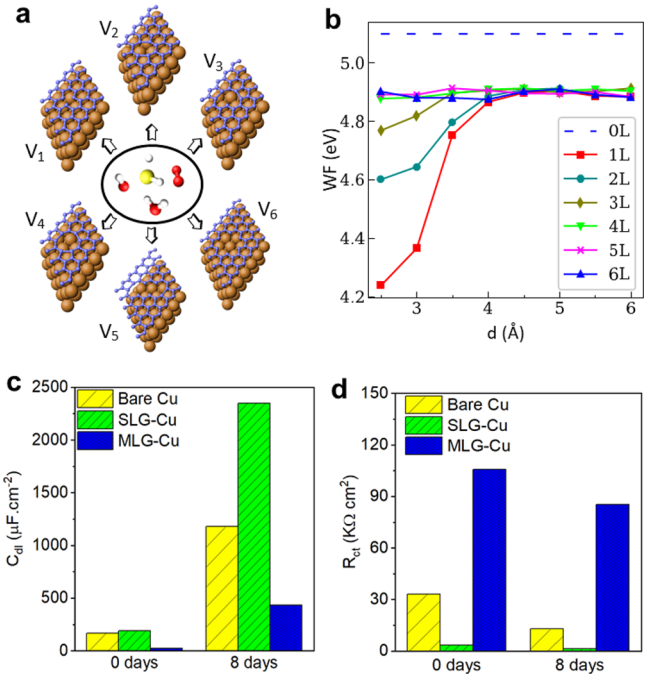

Figure 4. (a) Schematic of the defects in graphene that adsorb corrosive metabolites and enable their access to the underlying Cu surface. Inside the circle shows corrosive metabolic species of DA-G20. (b) Work function of Cu(111) surface with adsorbed few-layer (one to six layers) graphene as a function of graphene−Cu distance. Symbols show calculated values of W and a dashed blue line indicates the work function of bare Cu(111). (c) Double-layer capacitance of bare Cu, SLG-Cu, and MLG-Cu surface obtained from EIS analysis. (d) Charge-transfer resistance of bare Cu, SLG-Cu, and MLG-Cu surface obtained from EIS analysis.

pathways for the corrosive species (HS^-, H^+, OH^-, O_2, and H_2O) to permeate onto the underlying Cu surfaces. We used Cu (111) (6 layers of Cu atoms) modified with perfect graphene (1−6 layers) in the simulations. We evaluated the work function (WF) of SLG-Cu and MLG-Cu as a function of Cu−graphene distance (d), as depicted in Figure 4b. The computed value of WF (eV) for graphene-Cu (∼4.5 eV) is lower than that of bare Cu(111) (∼5.1 eV), and these values agree well with that of the previous report.[30]

Adsorbed graphene on Cu results in the formation of an electric double layer at the Cu−graphene interface. Our experimental results based on the electrochemical impedance spectroscopy (EIS) analysis suggest that SLG displays 100-fold higher double-layer capacitance (C_{dl}) compared to MLG (Figure 4c). As shown in Figure 4b, Cu−graphene displays the least value of WF when the number of graphene layers ranges from 1 to 3. Although the WF for SLG reduced only slightly from ∼5.1 to ∼4.9 eV at larger separation distances (d = 6 Å),

https://dx.doi.org/10.1021/acsnano.0c03987
ACS Nano 2021, 15, 447−454

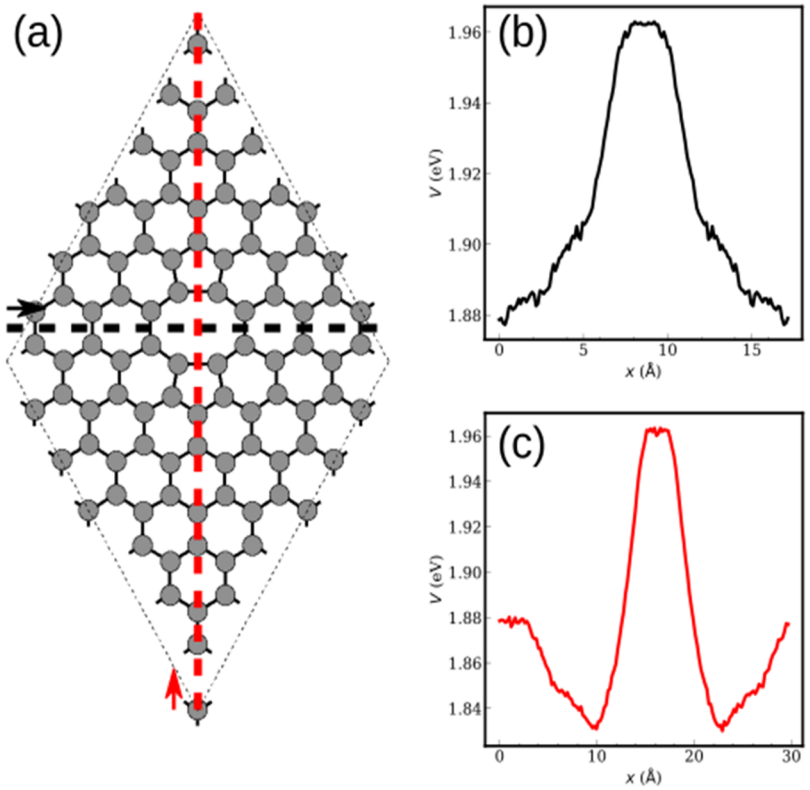

Figure 5. Electrostatic potential distribution near a point defect in graphene: (a) double vacancy in graphene; (b) potential for electrons along dashed horizontal line in (a) at a distance of 3 Å from the graphene plane; (c) potential for electrons along dashed vertical line in (a) at a distance of 3 Å from the graphene plane.

it dropped to ~4.6 eV at d = ~ 3.3 Å and to ~4.2 eV at d < 3.3 Å. For smaller values of d, WF decreases rapidly due to graphene−Cu chemical interactions as well as Pauli repulsion between the occupied graphene and Cu orbitals, pushing the electronic cloud into Cu, making Cu prone to corrosion. These interaction effects are largest for SLG-Cu, and such effects diminish with the increasing number of graphene layers, becoming negligible for MLG-Cu (>4 L). Thus, the fewer the number of graphene layers the higher the electrical double layer strength, lower the WF,[31,32] more electropositive the Cu, and higher the biotic corrosion.[20]

After establishing that SLG-Cu displays higher C_{dl} and lower WF, we describe that SLG-Cu donates electrons from the Cu oxidation and shifts the balance in eq 1 below toward the chemisorption of HS^- at the cathodic sites (defects).[20] Biotic corrosion begins with the attachment of DA-G20 cells on the Cu surfaces and subsequent growth into biofilm, as established in prior sections (Figure 2a). This biofilm releases corrosive metabolites that are strongly adsorbed onto inherent defects (Figure 4a),[33−35] which serve as cathodic sites for the galvanic corrosion of the underlying Cu surface. The excessive flow of biogenic HS^- to the cathodic sites is compensated by a rapid supply of electrons from the Cu oxidation.[36] The chemisorbed species further attack Cu to form Cu_2S deposits (Figure S1), promoting a biogenic sulfide attack (eq 2).

$$Cu + HS^- \rightarrow Cu(HS)_{ads} + e^- \quad (1)$$

$$Cu + Cu(HS)_{ads} + HS^- \rightarrow Cu_2S + H_2S + e^- \quad (2)$$

The H_2S from eq 2 is sorbed onto the edges of the nanoscale defects[33−35] to consume electrons from the Cu oxidation (eq 3).[34] Protons from the SRB metabolism also serve as the terminal electron acceptors to participate in the reduction reaction at the cathodic sites (eq 4).

$$2H_2S + 2e^- \rightarrow 2HS^- + H_2 \quad (3)$$

$$2H^+ + 2e^- \rightarrow H_2 \quad (4)$$

As seen in eqs 1−4, the lower the charge transfer resistance (R_{ct}) of HS^- on to the Cu surface, the higher will be the galvanic corrosion rates. The R_{ct} for SLG-Cu was at minimum 19-fold and 10-fold lower than for MLG-Cu and bare Cu, respectively, based on the EEC analysis (Figure S3) of the Nyquist data (Figure 4d). The effect of lower R_{ct} to Cu oxidation for SLG-Cu compared to bare Cu and MLG-Cu can be qualitatively observed in the Nyquist plots for day 0 (Figure 3c) and day 8 (Figure 3d), as indicated by the lowest semicircle diameter. Our results agree well with those from previous reports on the 10-fold higher electron mobility in SLG (23.3×10^4 $cm^2/V{\cdot}s$) *vs* MLG (2.0×10^4 $cm^2/V{\cdot}s$).[37,38] Moreover, the metabolites (HS^-, H^+) that increase over time act to dope the defects in graphene, as reflected in the temporal increase of values of C_{dl} and the corresponding decrease in R_{ct} to corrosion for both of the protective layer cases (Figure 4c,d), while according to density functional theory (DFT) calculations, the WF of Cu is lowered for any number of graphene layers making Cu more electropositive, electron tunneling between Cu and corrosive metabolites adsorbed on the outermost layer may be hindered for MLG-Cu. This would effectively slow down the reactions in eqs 1 and 2 and diminish the corrosion in MLG-Cu.

Next, we investigated the effect of atomic-scale vacancy defects and grain boundaries in graphene layers on their protection ability to underlying metals. We studied the effect of

https://dx.doi.org/10.1021/acsnano.0c03987
ACS Nano 2021, 15, 447−454

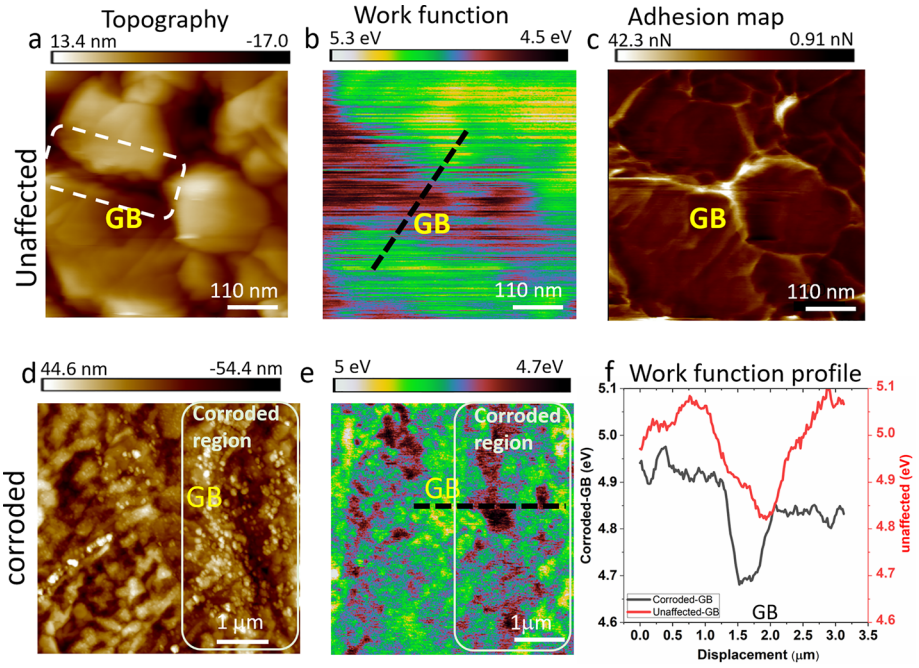

Figure 6. Effect of the grain boundaries in SLG-Cu. (a–c) Topography, WF, and adhesion force map of a pristine SLG-Cu. (d–f) Topography, WF map, and WF profile map for the exposed SLG-Cu (1 M H_2SO_4, 2h). (a) Different grain sizes oriented in random directions and the dashed rectangle shows a grain boundary (GB) region between two different grains. (b) Surface potential map and its associated WF of the GB are different from the surrounding grain, indicating different carrier concentrations at GB compared to grains. (c) Adhesion force between the metallic tip apex and the GB region is higher compared to the grain region. (d) AFM topography of an exposed-SLG/Cu (marked by a rectangle) and its corresponding WF map. (e) Presence of the corrodent particles decreases the WF at the GB compared to the grain region, in both the pristine (outside the rectangle) and exposed regions. (f) WF profile of the pristine grains and its GB, which is merged with partially corroded grains and its GB. The effect of corrosion is seen to be higher in the GB regions.

double-vacancy defects on the WF behavior of Cu(111) substrates modified with the atomic graphene layer (Figure 5). Typically, such defects locally change the WF of SLG-Cu, which in turn could affect the local corrosion rate. We calculated the electrostatic potential distribution near the double vacancy along the horizontal and vertical cuts at 3 Å above the graphene plane (Figure 5a) to quantify the change. We obtained a local perturbation of the potential, created by charge redistribution due to the formation of the defects and the perturbed field extends over distances of the order of vacancy size and has an amplitude of ∼80 meV at 3 Å above the plane. The larger potential energy for electrons near the defect means a larger change in the local WF, which would slow down the rate of electron removal during the oxidation step (Figure 5). A similar change in the WF behavior can also be expected for MLG-Cu structures, specifically near the defects in a top graphene layer of MLG-Cu.

After assessing the influence of vacancy defects, we studied the effect of grain boundaries (GB) on the corrosion resistance of SLG over Cu by Kelvin probe force microscopy (KPFM) analyses. The GB is indicated by a dashed white rectangle (Figure 6a) as marked between the two grains. Figure 6a–f shows the KPFM topography and WF distribution profile of a pristine region of the SLG-Cu sample as well as the region exposed to 1 M H_2SO_4 corrodent, specifically around the GB region. We chose H_2SO_4 as a model for aggressive corrodent as it prevails in anoxic microbial environments. Such acid metabolites result from oxidation of hydrogen sulfide (generated in eq 2) by SRB-mediated reactions:

$$2H_2S + 2O_2 \rightarrow H_2SO_4 \quad (5)$$

As shown in the WF profile (Figures 6f), the WF values in the GB region are significantly lower compared to its surrounding grains for both the pristine and exposed samples. The lower the WF the higher the tendency to donate the electrons and lower the corrosion resistance. However, such a drop in WF is higher for the exposed GB regions (∼4.68 eV) compared to their pristine counterparts (∼4.82 eV).

The adhesion force map or the work done by the metallic tip apex moving away from the surface is also higher at the GB regions (depicted by the bright regions in Figure 6c). This force map indicates the preferential surface chemistry of the GB toward the corrodent and the region of the exposed SLG-Cu (a solid line rectangle in Figure 6d) displays the presence of the salt impurities. To conclude, the GB in atomic graphene layers promote the higher charge injection tendency in SLG-Cu and a greater accumulation of the corrodent particles, suggesting the enhanced adhesive characteristics of GBs compared to the grains. Thus, grain boundaries can reduce the overall corrosion resistance of SLG on Cu.

Furthermore, we explored the protection ability of atomic graphene layers on other metals such as nickel (Ni) substrates (details are provided in Figures S5 and S6). We have carried out the DFT calculations to understand the WF behavior of SLG-Ni and MLG-Ni as a function of Ni-graphene distance (d). Also, we conducted a KPFM study to determine the WF of SLG-Ni and MLG-Ni substrates exposed to 1 M H_2SO_4 corrodent. Then, we conducted a comparative analysis by Raman Spectroscopy to study the doping and strain behavior of the SLG-Ni and SLG-Cu, for both pre- and postcorrosion conditions. The DFT analysis and KPFM study depicted lower WF of SLG-Ni compared to MLG-Ni, suggesting the greater

https://dx.doi.org/10.1021/acsnano.0c03987
ACS Nano 2021, 15, 447–454

activity of the electrons that participate in relevant electrochemical processes and lower (more negative) corrosion potential. Hence, MLG-Ni offers superior corrosion protection compared to SLG-Ni, similarly aligned with the findings from the Cu case (Figure 4). Raman studies confirmed that the atomic graphene layers on both Cu and Ni substrates stayed intact even after the prolonged exposure to the 1 M H_2SO_4 corrodent (Figure S7a,b). However, SLG-Ni displays a distinct deconvoluted strain and doping behavior compared to SLG-Cu at the pre- and postexposure conditions (Figure S7c) and suggests that SLG-Cu is more prone to corrosion compared to SLG-Ni, aligning with the results of the DFT simulations (Figure S5 and Figure 4, details in the Supporting Information).

CONCLUSIONS

In conclusion, metals used in biointerface applications are susceptible to microbial attack, a problem costing billions of dollars across the world. Although atomic graphene layers do not inhibit cell attachment and biofilm growth, they can effectively restrict the diffusion of aggressive metabolites to the underlying Cu surfaces and prevent biogenic sulfide attack. Owing to the small density of states, single-layered graphene displays distinct quantum capacitance effect and increases the electrical double layer capacitance and copper dissolution at the copper interfaces. This quantum capacitance effect decreases with the increase in the number of atomic graphene layers.[31] Thus, graphene coating should be designed rationally to minimize the impact of the capacitance effect, while taking into account the interplay between the inherent defects and the dynamics of inevitable biofilm growth and associated phenotypical and genotypic responses, all of which impact biogenic sulfide attack.

METHODS

A comprehensive description of the experimental procedures has been provided in the Supporting Information, and only a brief account is given below. Single-layer graphene (SLG) was grown on copper foil (25 μm thick) using a low-pressure chemical vapor deposition (LPCVD) at 1000 °C and 500 mTorr with a methane gas flow of 35 sccm. Multilayer graphene (MLG) was synthesized on copper foil (25 μm thick) by CVD at 940 °C under a pressure of 1.01×10^5 Pa and CH_4:H_2 flow ratio 10:30 (sccm) as described previously.[1] The CVD-grown SLG and MLG on copper foil (Bare Cu) are designated as SLG- Cu and MLG-Cu, respectively.

All electrochemical tests were carried out using a Gamry Reference 600 potentiostat. All of the tests were carried out using samples (bare Cu, SLG-Cu, and MLG-Cu) with an exposure area of 1 cm^2. The measurements were obtained after achieving steady-state OCP conditions. Microbial corrosion experiments were carried out in a 400 mL single compartment corrosion Cell Kit (Gamry Instruments) consisting of a graphite plate as a counter electrode, an Ag/AgCl as a reference electrode (RE), and the sample of interest as a working electrode (WE). The *D. alaskensis* strain G20 (DA-G20) that was anaerobically grown in the Lactate C (L-C) medium was used in all of the MIC experiments.

DFT calculations were performed using local density approximation (LDA) density functional, as implemented in the Quantum Espresso package.[39] Bernal (AB) stacking was used to model multilayer structures. In multilayer graphene, the z coordinate of the graphene layer nearest to the Cu surface was fixed, and all other coordinates were fully relaxed. Similarly, the z coordinate of the top layer of the Cu(111) slab was fixed, while other coordinates were fully relaxed. The equilibrium interlayer distance after the geometry optimization was 3.36 Å.

Kelvin probe force microscopy (KPFM): The KPFM investigations were performed using atomic force microscopy (AFM)-Bruker Dimension Icon. Peak-force KPFM through two pass modes has been used in the characterization; in the first pass, a topography image was collected, and the second pass for the potential map (contact potential difference, CPD). Conductive tip from Bruker (Model: PFQNE-Al, stiffness ≈ 0.8 ± 0.2 N/m, diameter ≈ 5 nm, resonance frequency = 300 kHz) has been used for the measurements. The calculation of the tip work function (WF) was carried out using freshly cleaved HOPG using the relation, $WF_{sample} = WF_{tip} - eV_{dc}$. The same relation is used to measure local WF of unaffected and corroded graphene.

The Raman spectroscopy was carried out with a 532 nm laser line, 1800 grating line/mm using the Renishaw inVia 100X optical lens. The laser power was limited to 5% (<1 mW) throughout the duration. The Raman peaks were fitted using the Lorentzian function to measure the peak positions for G and 2D peak.

ASSOCIATED CONTENT

Supporting Information

The Supporting Information is available free of charge at https://pubs.acs.org/doi/10.1021/acsnano.0c03987.

Optical, SEM, TEM, Raman, and contact angle analysis of SLG-Cu and MLG-Cu; preparation of sulfate-reducing bacterial (SRB) strain and its culture; microbial corrosion; electrochemical measurement; characterization of biofilms and corrosion deposits; EEC circuits; DFT calculations; protection ability of atomic graphene layers on Ni substrates; convoluted strain and doping effect behavior of graphene layers exposed to 1 M H_2SO_4; effects of surface roughness on corrosion behavior (PDF)

AUTHOR INFORMATION

Corresponding Authors

Pulickel M. Ajayan − *Department of Materials Science and NanoEngineering, Rice University, Houston, Texas 77005, United States;* orcid.org/0000-0001-8323-7860; Email: ajayan@rice.edu

Muhammad M. Rahman − *Department of Materials Science and NanoEngineering, Rice University, Houston, Texas 77005, United States;* orcid.org/0000-0003-1374-0561; Email: mr64@rice.edu

Venkataramana Gadhamshetty − *Department Civil and Environmental Engineering, South Dakota School of Mines and Technology, Rapid City, South Dakota 57701, United States; 2Dimensional Materials for Biofilm Engineering Science and Technology (2DBEST) Center, South Dakota School of Mines and Technology, Rapid City, South Dakota 57701, United States;* orcid.org/0000-0002-8418-3515; Email: venkata.gadhamshetty@sdsmt.edu

Authors

Govind Chilkoor − *Department Civil and Environmental Engineering, South Dakota School of Mines and Technology, Rapid City, South Dakota 57701, United States; 2Dimensional Materials for Biofilm Engineering Science and Technology (2DBEST) Center, South Dakota School of Mines and Technology, Rapid City, South Dakota 57701, United States*

Namita Shrestha − *Department of Civil and Environmental Engineering, Rose-Hulman Institute of Technology, Terre Haute, Indiana 47803, United States*

https://dx.doi.org/10.1021/acsnano.0c03987
ACS Nano 2021, 15, 447−454

Alex Kutana − *Department of Materials Science and NanoEngineering, Rice University, Houston, Texas 77005, United States;* orcid.org/0000-0001-6405-6466

Manoj Tripathi − *Department of Physics and Astronomy, University of Sussex, Brighton BN1 9RH, U.K.;* orcid.org/0000-0002-8052-428X

Francisco C. Robles Hernández − *Department of Materials Science and NanoEngineering, Rice University, Houston, Texas 77005, United States; Department of Mechanical Engineering Technology, University of Houston, Houston, Texas 770204, United States*

Boris I. Yakobson − *Department of Materials Science and NanoEngineering, Rice University, Houston, Texas 77005, United States;* orcid.org/0000-0001-8369-3567

Meyya Meyyappan − *Center for Nanotechnology, NASA Ames Research Center, Mountain View, California 94035, United States*

Alan B. Dalton − *Department of Physics and Astronomy, University of Sussex, Brighton BN1 9RH, U.K.;* orcid.org/0000-0001-8043-1377

Complete contact information is available at: https://pubs.acs.org/10.1021/acsnano.0c03987

Notes

The authors declare no competing financial interest.

ACKNOWLEDGMENTS

V.G. acknowledges funding support from the National Science Foundation CAREER award (No. 1454102), NSF RII T-1 FEC Award No. 1849206, NSF RII T-2 FEC Award No. 1920954, and NASA (No. NNX16AQ98A) for funding this research. P.M.A. acknowledges support from the Air Force Office of Scientific Research under Award No. FA9550-18-1-0072. Computational analysis (A.K. and B.I.Y.) was funded by the Department of Energy, Fossil Energy Program, UT-Battelle contract DE-AC05-00OR22725 via grant 4000174979, and by the R. Welch Foundation (C-1590).

REFERENCES

(1) Böhm, S. Graphene against Corrosion. *Nat. Nanotechnol.* **2014**, *9*, 741.
(2) Callow, M. E.; Callow, J. A. Marine Biofouling: A Sticky Problem. *Biologist* **2002**, *49*, 1−5.
(3) Kopteva, Z. P.; Zanina, V.; Kozlova, I. Microbial Corrosion of Protective Coatings. *Surf. Eng.* **2004**, *20*, 275−280.
(4) Bunch, J. S.; Verbridge, S. S.; Alden, J. S.; Van Der Zande, A. M.; Parpia, J. M.; Craighead, H. G.; McEuen, P. L. Impermeable Atomic Membranes from Graphene Sheets. *Nano Lett.* **2008**, *8*, 2458−2462.
(5) Liu, L.; Ryu, S.; Tomasik, M. R.; Stolyarova, E.; Jung, N.; Hybertsen, M. S.; Steigerwald, M. L.; Brus, L. E.; Flynn, G. W. Graphene Oxidation: Thickness-Dependent Etching and Strong Chemical Doping. *Nano Lett.* **2008**, *8*, 1965−1970.
(6) Prasai, D.; Tuberquia, J. C.; Harl, R. R.; Jennings, G. K.; Bolotin, K. I. Graphene: Corrosion-Inhibiting Coating. *ACS Nano* **2012**, *6*, 1102−1108.
(7) Xu, Y.; Qu, J.; Shen, Y.; Feng, W. Different Graphene Layers to Enhance or Prevent Corrosion of Polycrystalline Copper. *RSC Adv.* **2018**, *8*, 15181−15187.
(8) Tiwari, A.; Singh Raman, R. Long-Term Corrosion Protection of a Cupro-Nickel Alloy Due to Graphene Coating. *Coatings* **2017**, *7*, 210.
(9) Stoot, A. C.; Camilli, L.; Spiegelhauer, S.-A.; Yu, F.; Bøggild, P. Multilayer Graphene for Long-Term Corrosion Protection of Stainless Steel Bipolar Plates for Polymer Electrolyte Membrane Fuel Cell. *J. Power Sources* **2015**, *293*, 846−851.
(10) Su, Y.; Kravets, V.; Wong, S.; Waters, J.; Geim, A.; Nair, R. Impermeable Barrier Films and Protective Coatings Based on Reduced Graphene Oxide. *Nat. Commun.* **2014**, *5*, 4843.
(11) Chen, S.; Brown, L.; Levendorf, M.; Cai, W.; Ju, S.-Y.; Edgeworth, J.; Li, X.; Magnuson, C. W.; Velamakanni, A.; Piner, R. D. Oxidation Resistance Of Graphene-Coated Cu and Cu/Ni Alloy. *ACS Nano* **2011**, *5*, 1321−1327.
(12) Galbiati, M.; Stoot, A. C.; Mackenzie, D.; Bøggild, P.; Camilli, L. Real-Time Oxide Evolution of Copper Protected by Graphene and Boron Nitride Barriers. *Sci. Rep.* **2017**, *7*, 39770.
(13) Ahn, Y.; Jeong, Y.; Lee, D.; Lee, Y. Copper Nanowire−Graphene Core−Shell Nanostructure for Highly Stable Transparent Conducting Electrodes. *ACS Nano* **2015**, *9*, 3125−3133.
(14) Huang, Y.; Huang, Z.; Zhong, Z.; Yang, X.; Hong, Q.; Wang, H.; Huang, S.; Gao, N.; Chen, X.; Cai, D. Highly Transparent Light Emitting Diodes on Graphene Encapsulated Cu Nanowires Network. *Sci. Rep.* **2018**, *8*, 1−11.
(15) Xu, H.; Wang, H.; Wu, C.; Lin, N.; Soomro, A. M.; Guo, H.; Liu, C.; Yang, X.; Wu, Y.; Cai, D. Direct Synthesis of Graphene 3D-Coated Cu Nanosilks Network for Antioxidant Transparent Conducting Electrode. *Nanoscale* **2015**, *7*, 10613−10621.
(16) Yang, K.; Li, Y.; Tan, X.; Peng, R.; Liu, Z. Behavior and Toxicity of Graphene and Its Functionalized Derivatives in Biological Systems. *Small* **2013**, *9*, 1492−1503.
(17) Sanchez, V. C.; Jachak, A.; Hurt, R. H.; Kane, A. B. Biological Interactions of Graphene-Family Nanomaterials: An Interdisciplinary Review. *Chem. Res. Toxicol.* **2012**, *25*, 15−34.
(18) Xiao, X.; Li, Y.; Liu, Z. Graphene Commercialization. *Nat. Mater.* **2016**, *15*, 697−698.
(19) Li, X.; Cai, W.; An, J.; Kim, S.; Nah, J.; Yang, D.; Piner, R.; Velamakanni, A.; Jung, I.; Tutuc, E. Large-Area Synthesis of High-Quality and Uniform Graphene Films on Copper Foils. *Science* **2009**, *324*, 1312−1314.
(20) Huttunen-Saarivirta, E.; Rajala, P.; Carpén, L. Corrosion Behaviour of Copper under Biotic and Abiotic Conditions in Anoxic Ground Water: Electrochemical Study. *Electrochim. Acta* **2016**, *203*, 350−365.
(21) Jacobs, S.; Reiber, S.; Edwards, M. Sulfide-Induced Copper Corrosion. *J. - Am. Water Works Assoc.* **1998**, *90*, 62−73.
(22) Srivastava, A.; Galande, C.; Ci, L.; Song, L.; Rai, C.; Jariwala, D.; Kelly, K. F.; Ajayan, P. M. Novel Liquid Precursor-Based Facile Synthesis of Large-Area Continuous, Single, and Few-Layer Graphene Films. *Chem. Mater.* **2010**, *22*, 3457−3461.
(23) Kim, K. K.; Hsu, A.; Jia, X.; Kim, S. M.; Shi, Y.; Dresselhaus, M.; Palacios, T.; Kong, J. Synthesis and Characterization of Hexagonal Boron Nitride Film as a Dielectric Layer for Graphene Devices. *ACS Nano* **2012**, *6*, 8583−8590.
(24) Hsieh, Y.-P.; Hofmann, M.; Chang, K.-W.; Jhu, J. G.; Li, Y.-Y.; Chen, K. Y.; Yang, C. C.; Chang, W.-S.; Chen, L.-C. Complete Corrosion Inhibition through Graphene Defect Passivation. *ACS Nano* **2014**, *8*, 443−448.
(25) Kirkland, N.; Schiller, T.; Medhekar, N.; Birbilis, N. Exploring Graphene as a Corrosion Protection Barrier. *Corros. Sci.* **2012**, *56*, 1−4.
(26) Rafiee, J.; Mi, X.; Gullapalli, H.; Thomas, A. V.; Yavari, F.; Shi, Y.; Ajayan, P. M.; Koratkar, N. A. Wetting Transparency of Graphene. *Nat. Mater.* **2012**, *11*, 217.
(27) Li, J.; Wang, G.; Zhu, H.; Zhang, M.; Zheng, X.; Di, Z.; Liu, X.; Wang, X. Antibacterial Activity of Large-Area Monolayer Graphene Film Manipulated by Charge Transfer. *Sci. Rep.* **2015**, *4*, 1−8.
(28) Barbolina, I.; Woods, C.; Lozano, N.; Kostarelos, K.; Novoselov, K.; Roberts, I. Purity of Graphene Oxide Determines its Antibacterial Activity. *2D Mater.* **2016**, *3*, 025025.
(29) Banhart, F.; Kotakoski, J.; Krasheninnikov, A. V. Structural Defects in Graphene. *ACS Nano* **2011**, *5*, 26−41.
(30) Giovannetti, G.; Khomyakov, P.; Brocks, G.; Karpan, V. v.; Van den Brink, J.; Kelly, P. J. Doping Graphene with Metal Contacts. *Phys. Rev. Lett.* **2008**, *101*, 026803.

(31) Zhan, C.; Neal, J.; Wu, J.; Jiang, D.-e. Quantum Effects on the Capacitance of Graphene-Based Electrodes. *J. Phys. Chem. C* **2015**, *119*, 22297−22303.
(32) Naghdi, S.; Sanchez-Arriaga, G.; Rhee, K. Y. Tuning the Work Function of Graphene toward Application as Anode and Cathode. *J. Alloys Compd.* **2019**, *805*, 1117−1134.
(33) Reshak, A.; Auluck, S. Adsorbing H_2S onto a Single Graphene Sheet: A Possible Gas Sensor. *J. Appl. Phys.* **2014**, *116*, 103702.
(34) Faye, O.; Raj, A.; Mittal, V.; Beye, A. C. H_2S Adsorption on Graphene in the Presence of Sulfur: A Density Functional Theory Study. *Comput. Mater. Sci.* **2016**, *117*, 110−119.
(35) Borisova, D.; Antonov, V.; Proykova, A. Hydrogen Sulfide Adsorption on a Defective Graphene. *Int. J. Quantum Chem.* **2013**, *113*, 786−791.
(36) Cui, C.; Lim, A. T. O.; Huang, J. A Cautionary Note on Graphene Anti-Corrosion Coatings. *Nat. Nanotechnol.* **2017**, *12*, 834.
(37) Fang, X.-Y.; Yu, X.-X.; Zheng, H.-M.; Jin, H.-B.; Wang, L.; Cao, M.-S. Temperature-and Thickness-Dependent Electrical Conductivity of Few-Layer Graphene and Graphene Nanosheets. *Phys. Lett. A* **2015**, *379*, 2245−2251.
(38) Nagashio, K.; Nishimura, T.; Kita, K.; Toriumi, A. Mobility Variations in Mono-and Multi-Layer Graphene Films. *Appl. Phys. Express* **2009**, *2*, 025003.
(39) Giannozzi, P; Andreussi, O; Brumme, T; Bunau, O; Buongiorno Nardelli, M; Calandra, M; Car, R; Cavazzoni, C; Ceresoli, D; Cococcioni, M; Colonna, N; Carnimeo, I; Dal Corso, A; de Gironcoli, S; Delugas, P; DiStasio, R A; Ferretti, A; Floris, A; Fratesi, G; Fugallo, G; Gebauer, R; Gerstmann, U; Giustino, F; Gorni, T; Jia, J; Kawamura, M; Ko, H-Y; Kokalj, A; Kucukbenli, E; Lazzeri, M; Marsili, M; Marzari, N; Mauri, F; Nguyen, N L; Nguyen, H-V; Otero-de-la-Roza, A; Paulatto, L; Ponce, S; Rocca, D; Sabatini, R; Santra, B; Schlipf, M; Seitsonen, A P; Smogunov, A; Timrov, I; Thonhauser, T; Umari, P; Vast, N; Wu, X; Baroni, S Advanced Capabilities for Materials Modelling with Quantum ESPRESSO. *J. Phys.: Condens. Matter* **2017**, *29*, 465901.

https://dx.doi.org/10.1021/acsnano.0c03987
ACS Nano 2021, 15, 447−454